Available online at www.sciencedirect.com
ScienceDirect
Computers & Graphics 32 (2008) 268–281
COMPUTERS & GRAPHICS
www.elsevier.com/locate/cag

Chaos and Graphics

Truchet curves and surfaces

Cameron Browne

SWiSHzone.com Pty Ltd., The Basement, 33 Ewell Street, Balmain 2041, Australia

Abstract

Spanning tree contours, a special class of Truchet contour based upon a random spanning tree of a Truchet tiling's underlying graph, are presented. This spanning tree method is extended to three dimensions to define a Truchet surface with properties similar to its two-dimensional counterpart. Both contour and surface are smooth, have known minimum curvature and known maximum distance to interior points, and high ratios of perimeter to area and area to volume, respectively. Expressions for calculating contour length, contour area, surface area and surface volume directly from the spanning tree are given.

Keywords: Truchet tile; Truchet contour; Spanning tree contour; Truchet surface; Area- and space-filling curves and surfaces

1. Introduction

French clergyman Sébastien Truchet (1657–1729) is best known for two mathematical innovations; the invention of the point system for measuring the size of typographic characters, and his description of a certain type of artistic tiling. In a short paper titled "Memoir sur les Combinaisons" published in 1704, Truchet described a ceramic tile he had recently seen consisting of a square divided by a diagonal line between opposite corners into two coloured parts [1], and went on to provide a combinatorial analysis of the many aesthetically interesting patterns that can be created with the four possible orientations of such a tile (Fig. 1, top left). Although Truchet's analysis focussed on structured nonrandom designs, tilings formed by filling a square grid with random integers from {0, 1, 2, 3} and substituting the appropriate tile can still be aesthetically interesting (Fig. 1, bottom left).

In his 1987 description of Truchet's tiles, metallurgist and historian Cyril Stanley Smith described the tile variation shown in Fig. 1 (top right) consisting of two circular 90° arcs with radius equal to half the tile width and centred at opposite corners [1]. Random tilings of this modified tile in its two possible orientations form visually interesting results [2,3]. The term *Truchet tiling* has been popularly adopted to refer to this modified form of tiling.

Truchet tiles have been used by many artists and rendered in various styles over recent years, some of which are shown Fig. 2. The leftmost design is a *duotone* pattern consisting of two unique tiles each of which have two orientations. Each tile placement is a free choice but must be oriented so that its edge colours match those of existing neighbours. Fig. 2 (middle) shows a *tritone* pattern consisting of three tiles with four orientations each. This design's regularity is no coincidence as placement is much more limited in this case—for each tile to be placed adjacent to two existing tiles, only one particular tile in one particular orientation will match edge colours with both neighbours. Fig. 2 (right) shows colour-coding of the continuous paths formed by a Truchet tiling. Each path is assigned a random colour for decorative purposes.

2. Truchet contours

A number of disjoint simple closed curves will tend to form in Truchet tilings, such as the red and gold curves in Fig. 2 (right). Such curves are described as *Truchet contours* by Gale et al. [4] and, like any other simple closed curve, will have clearly defined inside and outside regions in accordance with the Jordan Curve Theorem [5]. Fig. 3

E-mail address: Cameron.Browne@swishzone.com

0097-8493/$ - see front matter © 2007 Elsevier Ltd. All rights reserved.
doi:10.1016/j.cag.2007.10.001

shows the three simplest Truchet contours: the circle and the left and right dumbbell shapes.

Alan Tonisson, a researcher at Canon Information Systems Research Australia (CISRA), shows how to calculate the expected number of circles E_c and dumbbells E_d that will occur in a random $m \times n$ tiling, based on an observation by mathematician Torsten Sillke [6]. Given P_0 and P_1 the probabilities of tile 0 or tile 1 occurring at a given position (which will both be 0.5 for a random tiling), the expected frequencies will be

$$\begin{aligned} E_c &= (m-1)(n-1)P_0^2P_1^2 \\ &= (m-1)(n-1)0.5^20.5^2 \\ &= (m-1)(n-1)0.0625, \end{aligned} \tag{1}$$

$$\begin{aligned} E_d &= (m-2)(n-2)(P_0^5P_1^2 + P_0^2P_1^5) \\ &= (m-2)(n-2)(0.5^50.5^2 + 0.5^20.5^5) \\ &= (m-2)(n-2)0.00781. \end{aligned} \tag{2}$$

These equations are based on the observation that the circle pattern requires two 0-tiles and two 1-tiles, the left dumbbell requires five 0-tiles and two 1-tiles, while the right dumbbell requires two 0-tiles and five 1-tiles. Further, if the $m \times n$ tiling is continous and wraps around each border in toroidal fashion then these equations can be simplified to

$$E'_c = mnP_0^2P_1^2 \quad (\text{for } m>1 \text{ and } n>1), \tag{3}$$

$$E'_d = mn(P_0^5P_1^2 + P_0^2P_1^5) \quad (\text{for } m>2 \text{ and } n>2). \tag{4}$$

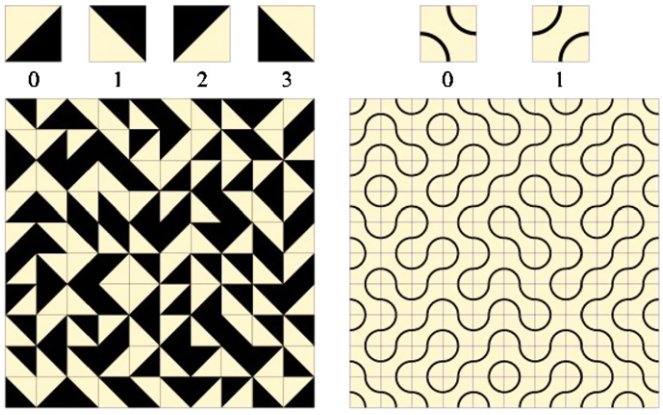

Fig. 1. Truchet's original tiles (left) and their popular incarnation (right).

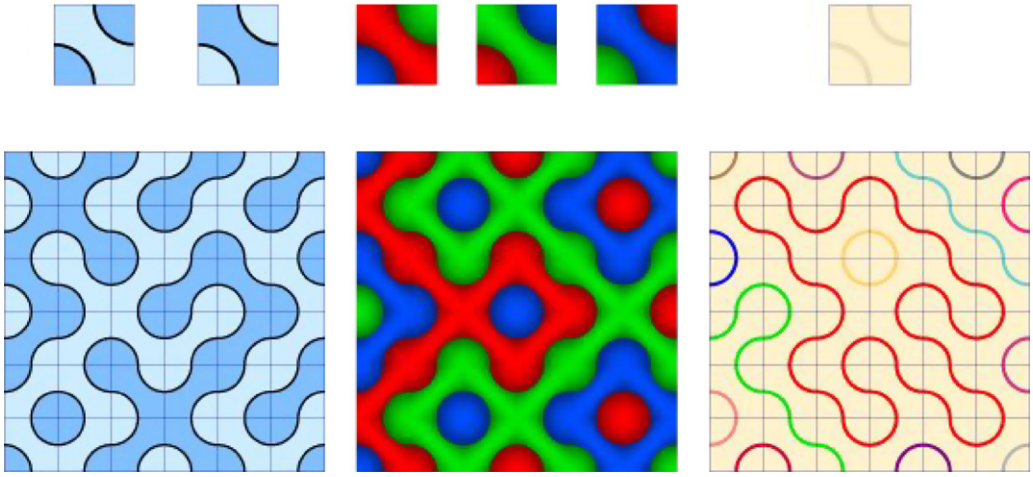

Fig. 2. Different styles: duotone, tritone and path colouring.

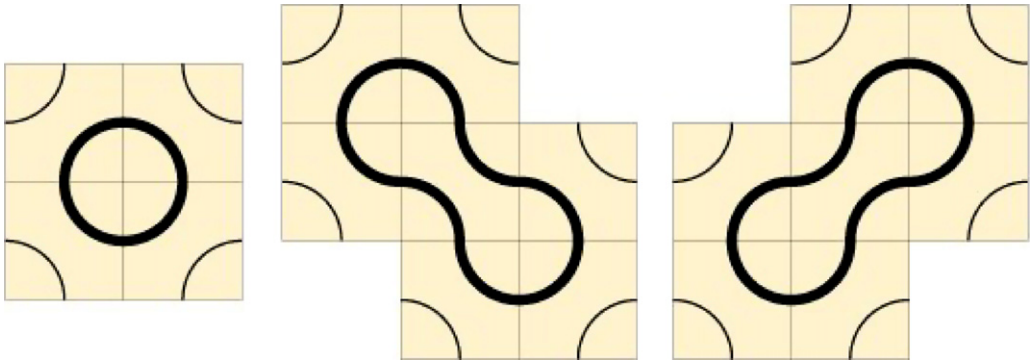

Fig. 3. The simplest Truchet contours: circle, left dumbbell and right dumbbell.

3. Spanning tree (ST) contours

It is sometimes desired to fill an area of a specific shape with a single uninterrupted curve. This may be for practical reasons, such as path-planning for automated embroidery equipment, or for purely artistic reasons. Truchet contours provide a convenient and attractive way to achieve this goal.

Listing 1 describes an algorithm for generating the minimum number of Truchet contours that will fill a given area to a specified resolution. This minimum number will be one unless the area is too small to support a 2×2 set of cells or contains regions of degenerate geometry as explained in the next section.

Figs. 4–6 demonstrate this algorithm by way of example. Fig. 4 (left) shows a grid of square cells whose midpoints

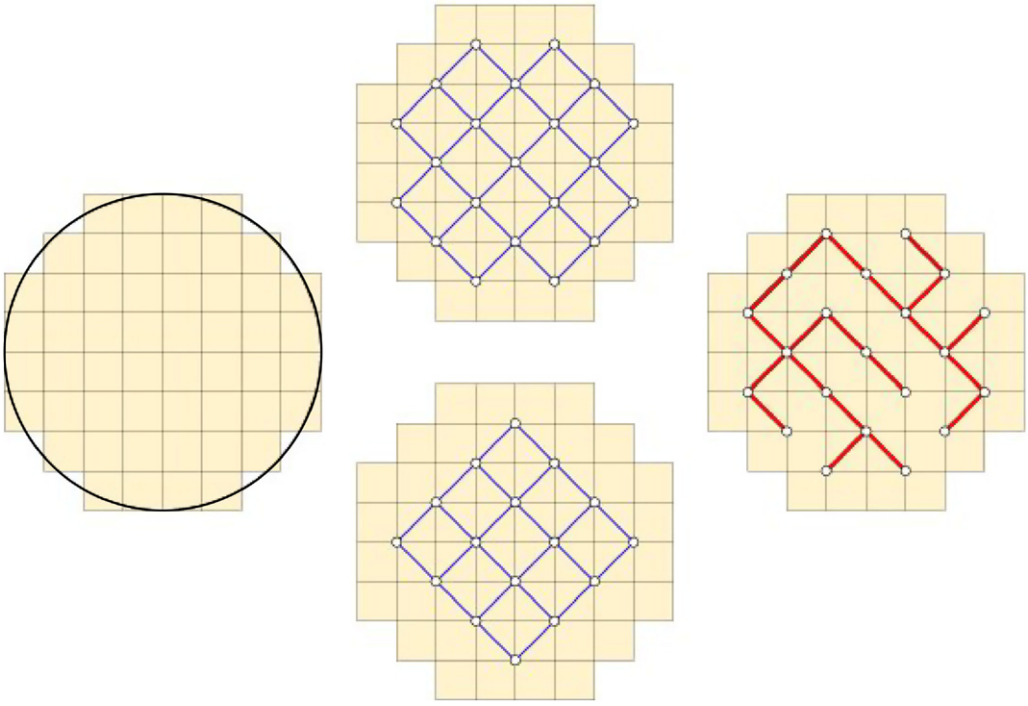

Fig. 4. Grid of cells filling a source shape (circle), two corresponding graphs and a spanning tree.

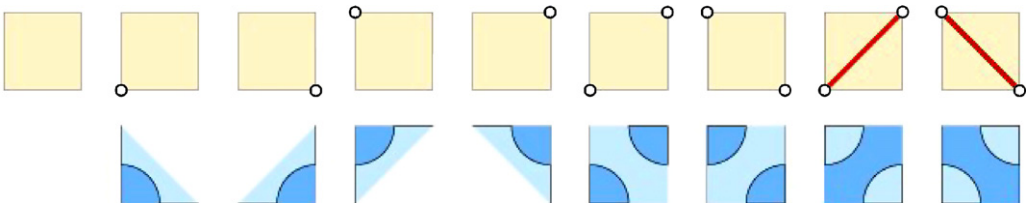

Fig. 5. Tree-to-contour replacement rules.

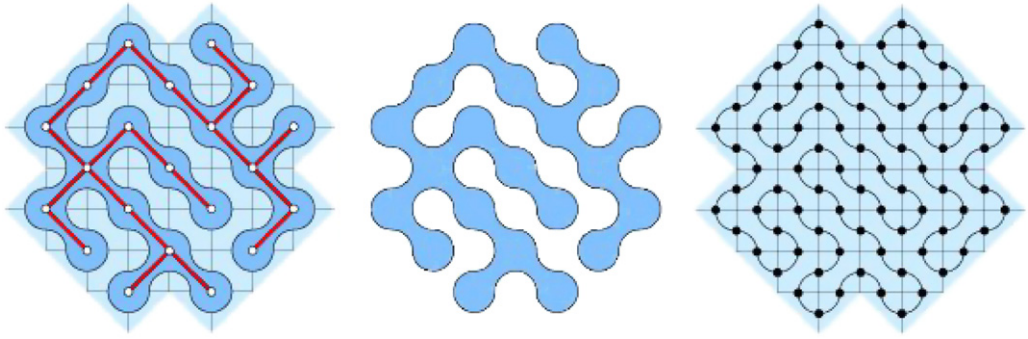

Fig. 6. Closed contour with graph overlaid, the final shape and the hamiltonian cycle within its footprint.

fall within a target area (a circle in this case). Fig. 4 (middle) shows two connected undirected graphs formed by placing vertices with diagonal adjacency at alternating 2×2 intersections, with adjacencies marked in blue.

There will generally be two such graphs of different size for a given target shape, distinguished by parity as G_0 and G_1; select G the larger of G_0 and G_1 (the upper graph in this case). Fig. 4 (right) shows a spanning tree of G chosen at random from all possible spanning trees of G using Broder's algorithm [7]. Edges of the spanning tree are marked in red. As with any tree, the number of edges E will be one less than the number of vertices V:

$$E = V - 1. \tag{5}$$

Fig. 5 shows the replacement rules used to create a single Truchet contour from a spanning tree. The top row shows the possible states for each visited cell, which may include zero, one or two vertices and zero or one edges. The bottom row shows the corresponding 90° arcs that will form the contour boundary within each cell. Dark blue regions indicate areas that will be inside the resulting contour and light blue regions indicate areas that will be outside the contour but within its *footprint* (effectively the contour's complement). The two edge rules (rightmost) are reminiscent of Duplantier's diagonal and antidiagonal bonds for performing hull percolation [8].

Fig. 6 shows the resulting contour and its footprint with the spanning tree overlaid (left) and the final shape (middle). The contour fills the target area with a single, simple closed curve that forms a hamiltonian circuit passing through the midpoint of every lattice edge within its footprint exactly once (right). Contours developed with this technique are called *spanning tree (ST) contours* to distinguish them from general Truchet countours. No ST contour will contain any holes or smaller contours, regardless of the target shape's topology.

Fig. 7 shows two higher resolution ST contours fitted to more complex shapes. The comma shape with the eye (right) demonstrates the no-hole property of the resulting contour, as a path can be traced from the comma's eye to its exterior without crossing the contour; ST contours have an immediate application in the design of mazes. In fact, Truchet-style tiles are used as the basis for several strategy games including Trax [9], Meander and the Black Path Game [10], all of which predate Smith's seminal 1987 article that associates such tiles with the work of Sébastien Truchet.

4. Contour characteristics

Given r, the radius of the contour's 90° arcs (which will be half the unit cell size), the perimeter length and area of a given ST contour can be calculated directly from V the number of vertices in its underlying graph.

Notice that the rightmost four replacement rules for cells with two vertices in Fig. 5 generate arc pairs of equal length regardless of whether the two vertices are connected by an edge or not. Cutting all edges of the spanning tree as shown in Fig. 8 (left) will not affect the contour's length L_{tc}, which can therefore be calculated from the number of vertices V as follows:

$$L_{tc} = 2prV. \tag{6}$$

The contour's area A_{tc} can similarly be calculated directly from the spanning tree. Each vertex will contribute the area of a circle of radius r, and each edge will contribute the area of a $2r \times 2r$ cell minus the area of four quarter circles of radius r, as shown in dark blue in Fig. 8 (right). From

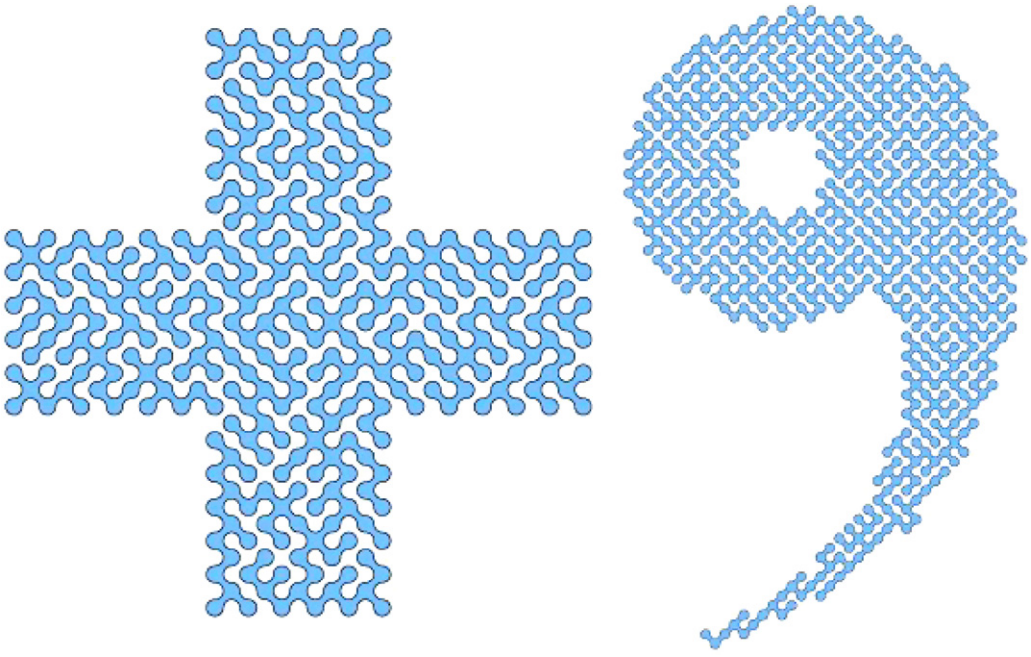

Fig. 7. More detailed ST contours.

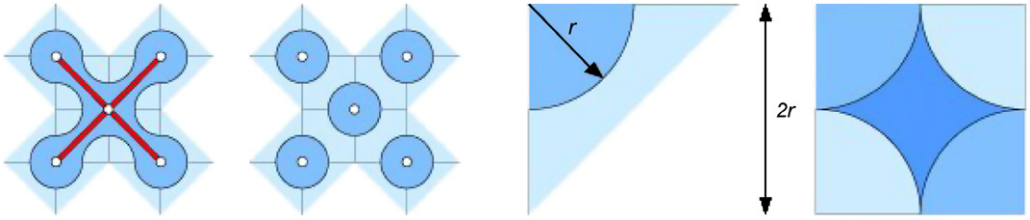

Fig. 8. Cutting edges to determine perimeter length (left) and basic area considerations (right).

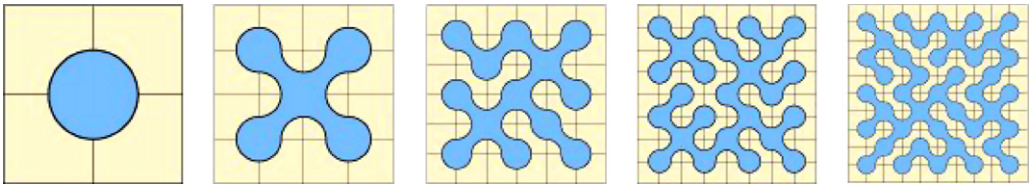

Fig. 9. ST contours for even-sided grids 2×2, 4×4, 6×6, 8×8 and 10×10.

Eq. (5) the number of edges will be $V-1$, hence

$$\begin{aligned} A_{tc} &= V\pi r^2 + E((2r)^2 - \pi r^2) \\ &= V\pi r^2 + (V-1)(4r^2 - \pi r^2) \\ &= r^2(V\pi + (V-1)(4-\pi)) \\ &= r^2(4V - 4 + \pi). \end{aligned} \tag{7}$$

Fig. 9 shows ST contours fitted to unit square grids with an even number of cells per side in order to demonstrate the relationship between length, area and grid resolution (odd-sided square grids result in two unused cells that complicate matters unduly). It can been seen that the boundary's length and convolution continue to increase with increasing iterations while the contour area remains reasonably constant.

The relationship between length and area is shown graphically in Fig. 10 with plots of perimeter length and contour area (as a percentage of total grid area) for increasing grid resolutions. Contour area approaches a limit of 50% of the total grid area while perimeter length continues to increase (interestingly, this rate of increase approaches π). The fact that the contour area approaches a limit of 50% is based on the observation that $V = 2n^2-2n+1$ for $2n\times2n$ grids, hence A_{tc} will approach $8n^2r^2$ as resolution approaches infinity, while the total grid area will be $(2n\times2r)^2 = 16n^2r^2$.

ST contours therefore provide a high ratio of length to area, especially for higher resolution grids. Other attractive properties include the facts that the curvature of the boundary will never exceed $1/r$ at any point, and that any point within the contour or its footprint will never be further than r distance from the boundary. The contour's footprint will have similar properties, and the areas of contour and footprint will be similar but never identical.

Turning now to the effect of pathological cases upon the algorithm, Fig. 11 (left) shows a target area consisting of

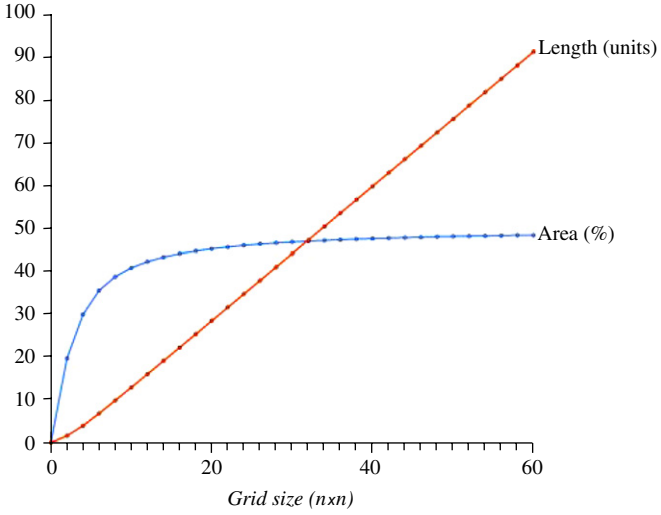

Fig. 10. Graph of contour perimeter and area for even-sided grids up to 60×60.

two regions joined by a *bottleneck* two cells wide. Neither G_0 nor G_1 can pass this bottleneck, which effectively cuts the grid into two component regions that must be filled separately with two distinct contours. Both contours in this case are of equal length and area (they both have the same number of vertices), however, the left contour visits fewer cells (22 as opposed to 24) even though both footprints are of equal size ($10+12/2 = 16$ and $8+16/2 = 16$). The right contour is visibly the better fit of the pair, and in any choice between two graphs of equal size the one that visits the most cells should be chosen.

Fig. 11 (right) shows a region with two potential bottlenecks. Either bottleneck can be traversed depending on the graph's parity but not both bottlenecks within the same parity. The algorithm identifies the largest possible graph to be the one that traverses the left bottleneck; this contour is fitted first, then the smaller one is fitted. The

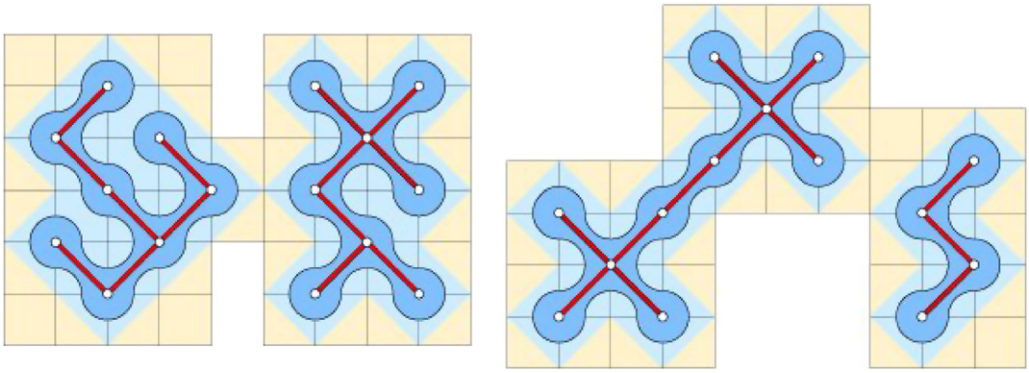

Fig. 11. Impassable bottlenecks split the contour.

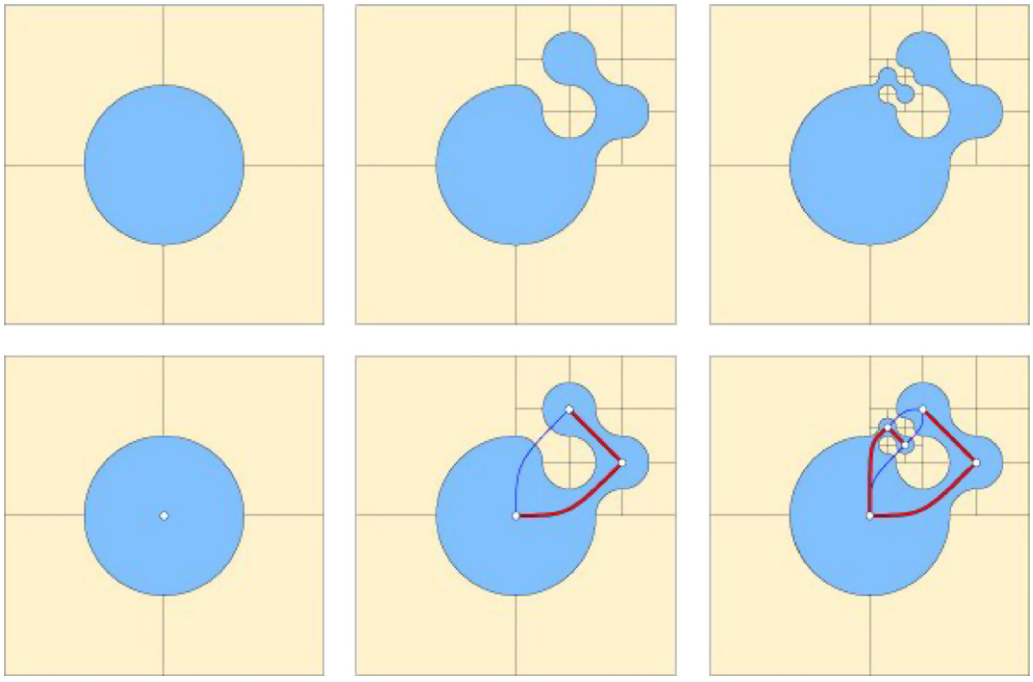

Fig. 12. Multiresolution ST contours (top row) and their corresponding graphs (bottom row).

parity of disjoint contours need not be the same, and is in fact different in this case.

The algorithm is greedy as it fits the largest possible contour with each iteration. This produces good results in practice, though it is conceivable that the number of contours may be further improved by combinatorial analysis in some rare pathological cases.

5. Multiresolution ST contours

So far the contours have been based upon grids of uniform resolution. Fig. 12 demonstrates how the algorithm can be adapted to generate more complicated contours based upon multiresolution grids.

Starting with a quadtree formed by a basic 2×2 square grid (left) the top right cell is subdivided into a nontree of nine equal sub-cells and the 90° arc for this cell reshaped into eleven 90° sub-arcs to fit the finer grid (middle). This process is then repeated to generate sub-sub-arcs to fit a sub-sub-cell (right).

The corresponding graphs for each figure, shown on the bottom row, reveal the underlying structure of the subdivided contour. Each subdivision creates two adjacencies from the larger scale vertex to two vertices of smaller scale cells and an adjacency between them. A spanning tree is found and tree-to-contour replacement rules again applied, with additional rules to handle the split adjacency between vertices of different scale (these rules can be deduced from the figure).

Multiresolution ST contours provide a convenient way to halftone digital images with a single closed curve. Starting with a quadtree of 2×2 cells mapped to the area of a source image, cells are subdivided if the total number of black pixels within the corresponding area of the image exceeds a certain threshold (25% in this case). Cells are recursively subdivided until a specified level of detail is

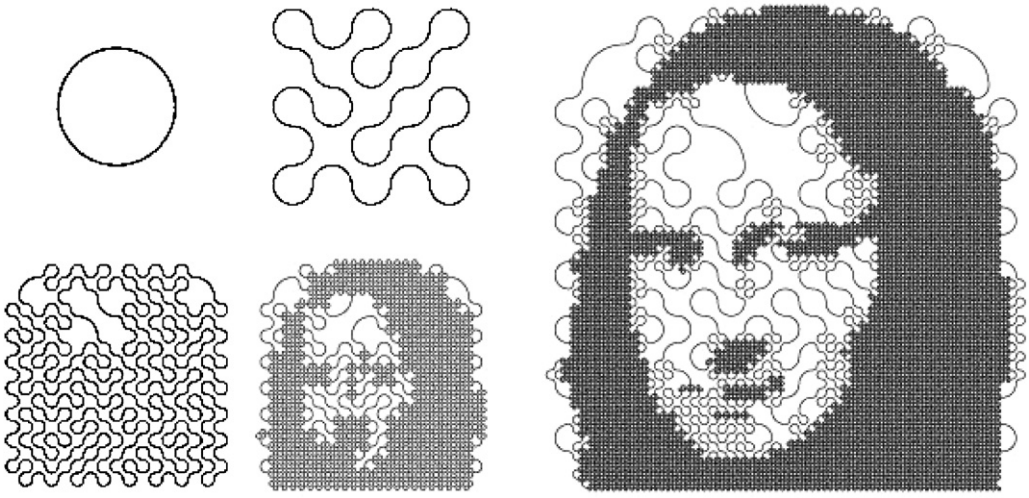

Fig. 13. Halftoning by multiresolution ST contour. Each step produces a single curve.

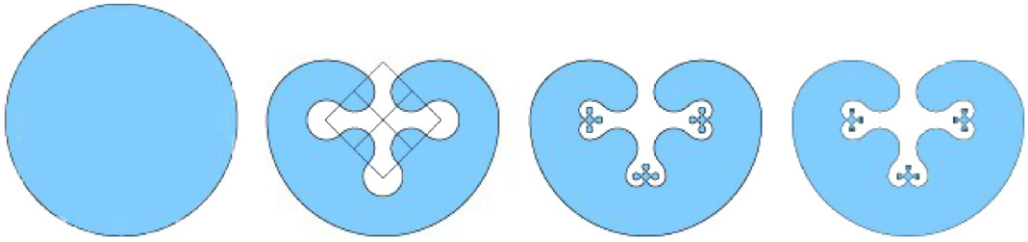

Fig. 14. Three iterations of the kidney fractal.

reached. Fig. 13 shows the first five levels of subdivision for the image of a familiar face, each composed of a single contour. The resulting halftone patterns are reminiscent of Bosch and Herman's travelling salesman problem (TSP) art [11]. In fact, ST contours provide a weak solution to the travelling salesman problem by visiting all lattice edge midpoints within the contour's footprint exactly once with a single path.

Fig. 14 shows a kidney-shaped fractal design using a multiresolution approach in which the contour is modified with inverted clover shapes at 1/9th scale with each iteration. The square grid overlaid in the second figure shows that each clover shape is based upon Truchet tiles of the appropriate size; the figure is entirely composed of circular arcs.

6. Truchet tiling in three dimensions

The Tangle, a manipulative puzzle from the 1970s composed of plastic 90° arcs that may be clipped together at various angles to create closed space loops [12], suggests a natural way to extend Truchet tiling to three dimensions. Fig. 15 (left) shows two unit cubes with the midpoints of adjacent faces joined by such 90° space arcs, as opposed to the 90° plane arcs that join adjacent sides of square two-dimensional Truchet tiles. Fig. 15 (right) shows a packing of such unit cubes, randomly chosen and oriented, to fill space and produce convoluted space curves [13,14] which may be called *Truchet pipes*.

While some Truchet pipes will form closed loops, the clear distinction between inside and outside to be found in Truchet contours is lost. To achieve this distinction, the three-dimensional design must be modified to produce a surface rather than a number of space curves, as shown in Fig. 16. The left column shows two cubes marked with Truchet tiles on each face in different rotational combinations, the middle column shows the underlying graphs with edges between diagonally connected vertices, and the right column shows the resulting surface patches. Adjacent sides of the cube are therefore joined by surface patches with 90° arc profiles rather than 90° arcs themselves.

It is tempting to assemble such unit cube surface patches in random combinations (but with each face matching the tile orientation of its neighbour) to construct larger surfaces, however a serious problem occurs. It can be seen in Fig. 16 (lower right) that the surface patches of two or more connections meeting at a common vertex overlap to form creases rather than joining smoothly. This is because the diagonal nature of adjacency along each face means that four corners of each cube form a tetrahedron of potential connection, and the coincident connections will meet at less than 90° as the dihedral angle of the tetrahedron is $acos(1/3) \approx 70.528779°$. These creases may be smoothed, for instance using Ken Brakke's Surface

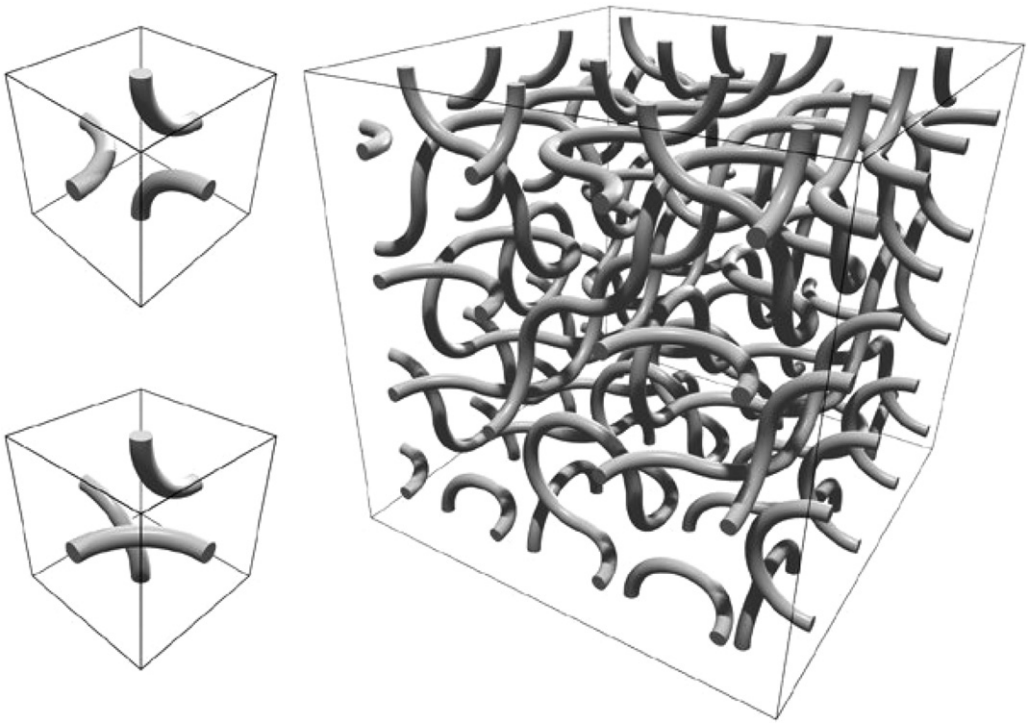

Fig. 15. Three-dimensional Truchet pipes.

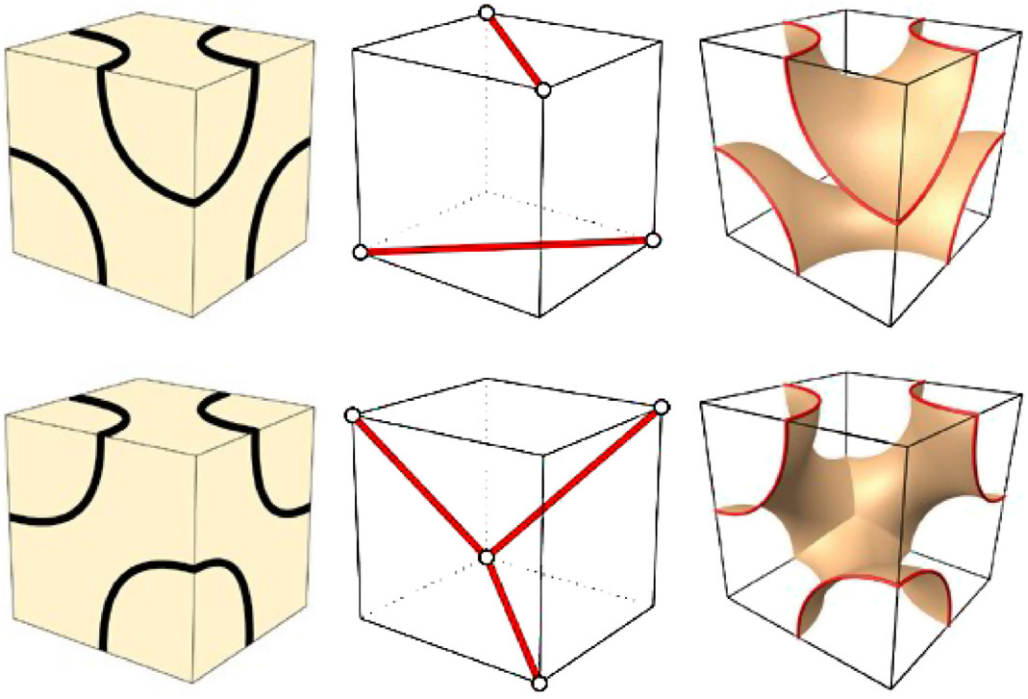

Fig. 16. Two Truchet-tiled cubes, their underlying graphs and the resulting surface patches.

Evolver software [15], however the shape of the resulting surface becomes implementation-dependent and less clearly defined.

One solution is to stipulate that each potential connection point support at most one connection, meaning that any cube with two connections would be of the form shown in Fig. 16 (top row) and that no cube would have more than two connections. This would remove the problem of creases but result in a sparser fill as a maximum of only four connections could meet at any point (rather than twelve in the fully connected case). A better solution is to reorient connections to join orthogonal rather than

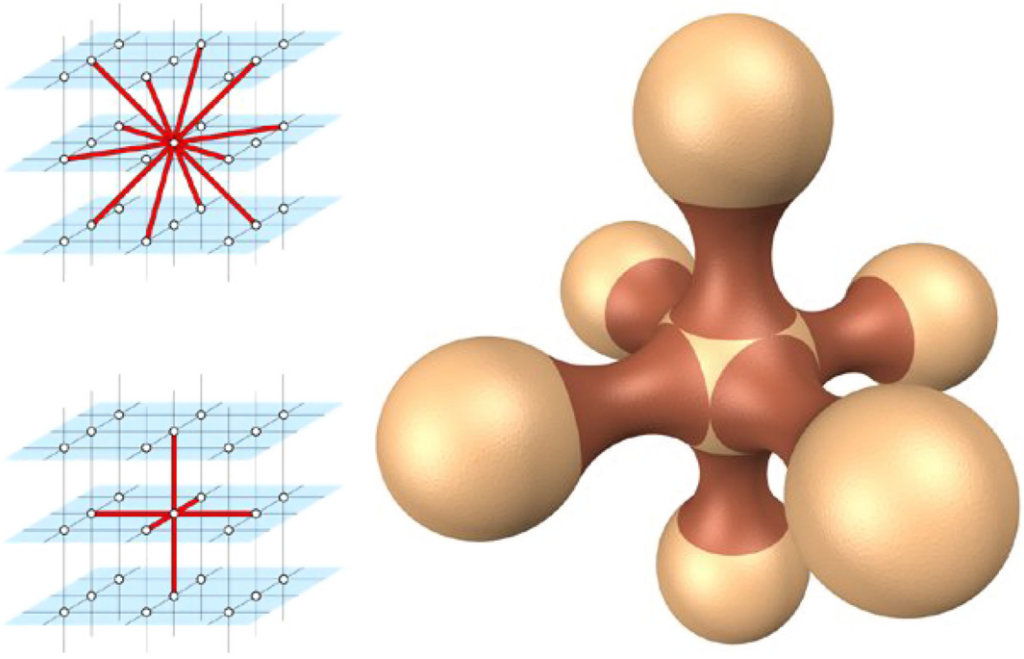

Fig. 17. Diagonal and orthogonal lattice adjacencies (left) and an orthogonally based Truchet surface (right).

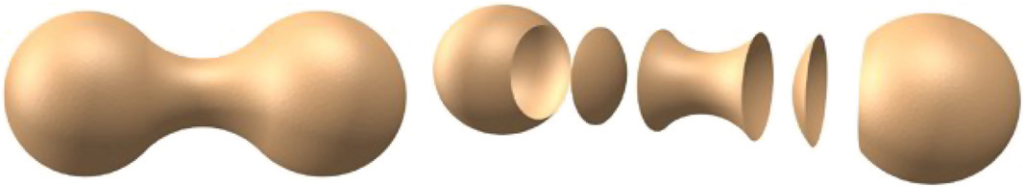

Fig. 18. A three-dimensional dumbbell and its component parts: 2 spheres + 1 neck − 2 caps.

diagonal neighbours in the cubic lattice, as shown in Fig. 17. This allows a maximum of six potential connections at each vertex (left) and means that surface patches at all such maximally connected vertices join smoothly at 90° (right) to form a *Truchet surface*.

7. Truchet surface construction

Fig. 18 (left) shows the Truchet surface formed by two spheres joined by a *neck*. This surface is similar to a shape called the Cassini oval, but is actually the surface of revolution formed by the ubiquitous dumbbell shape, and is the building block of the Truchet surface. Fig. 18 (right) shows its component parts: two spheres, a neck and the two spherical caps sliced off where the neck joins each sphere. The sphere centres must lie $2\sqrt{2}r$ units apart to ensure that the neck's maximum curvature ($1/r$) matches that of the spheres.

Listing 2 shows how this Truchet surface may be described as a constructive solid geometry (CSG) object in the POV-Ray public domain ray tracing language. Each spanning tree vertex corresponds to a sphere and each edge corresponds to a neck formed by the difference between a cylinder joining the two spheres and a torus enclosing it. The radius of the cylinder equals the neck's maximum radius ($\sqrt{2}r$) and the inner radius of the torus's hole equals the neck's minimum radius at its middle ($\sqrt{2}r/2$). The entire surface is consolidated by a merge operation rather than a union so that superfluous regions such as the cylinder's ends and the spherical caps formed at junctions are removed from the surface's interior. More complex surfaces may be described simply by merging the required number of spheres and necks, positioned and rotated as appropriate.

Truchet surfaces can be constructed using the spanning tree approach outlined in Section 3, except that the base lattice must be cubic rather than square and the tree-to-surface replacement rules modified to create a sphere for each vertex and a neck for each edge. In addition, there is no need to test which parity is best as potential adjacencies will coincide with lattice edges and there will be only one possible fit for orthogonal connections. The surface's spanning tree representation translates directly to its POV-Ray description.

Fig. 19 (left) shows a Truchet surface fitted to a $4 \times 4 \times 4$ cubic lattice with a spacing of $2\sqrt{2}r$ units. It can be seen that axial slices through the surface at unit intervals reveal cross-sectional sets of Truchet (but not necessarily ST)

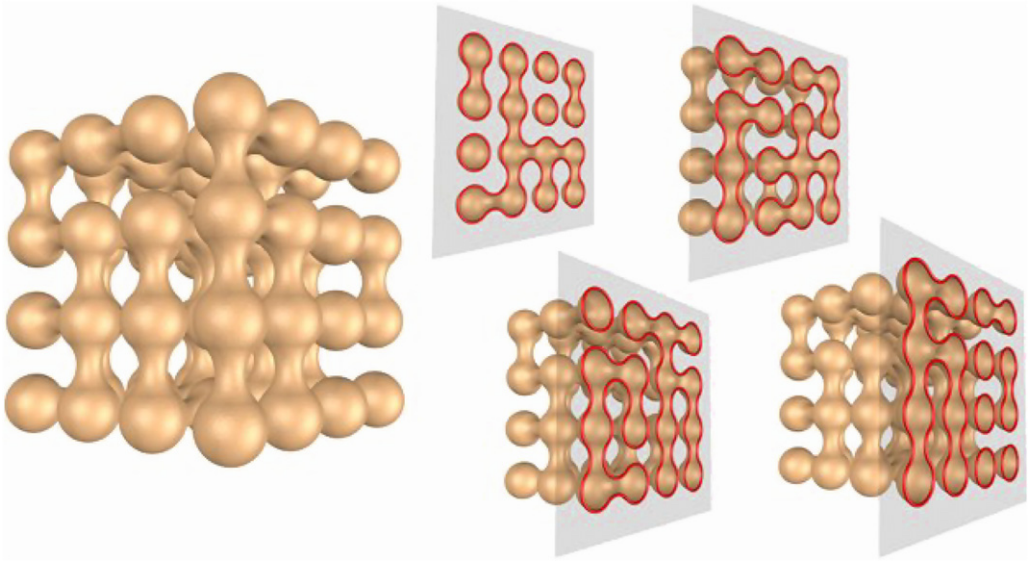

Fig. 19. Axial slices through the surface reveal Truchet contours at each unit interval.

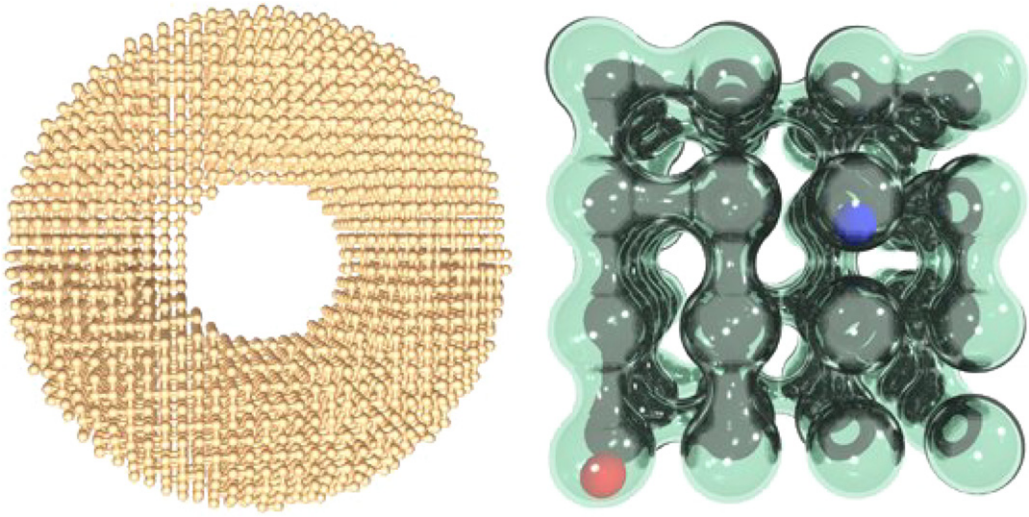

Fig. 20. A Truchet surface filling a torus with 6120 vertices and a Truchet glass bead puzzle.

contours. This will be the case whether the slices are made perpendicular to the x, y or z directions.

Fig. 20 (left) shows a Truchet surface formed from a higher resolution lattice fitted to the volume of a torus. This surface is composed of 6120 vertices giving 6120 spheres and 6119 necks. Fig. 20 (right) shows a possible design for a hollow glass bead puzzle containing two beads small enough to move through the necks, based on the $4 \times 4 \times 4$ Truchet surface of Fig. 19. The aim is to use gravity to manipulate the two beads so that they touch and then to move them apart to opposite corners of the grid (this would not be possible if the surface had a diagonal basis). A more difficult requirement would be to move the beads to every possible pair of corners while making them touch in between. Such a puzzle would be something of a glass-blowing challenge, and would also be quite fragile as the ST-based design lacks cycles which may act as supports, hence any shearing or torsional force must effectively be absorbed by a single glass neck.

Fig. 21 shows the development of a multiresolution Truchet surface by reducing a neck to one third of its diameter to join the protruding neck of a $3 \times 3 \times 3$ sub-surface. This development gives a smooth join between generations, but is not as elegant as the multiresolution ST contour since the parent shape must be modified to meet its children.

8. Surface characteristics

As with the two-dimensional case, Truchet surfaces are simple, smooth and closed, have clearly defined inside and outside regions, no holes or loops (they are genus 0) and

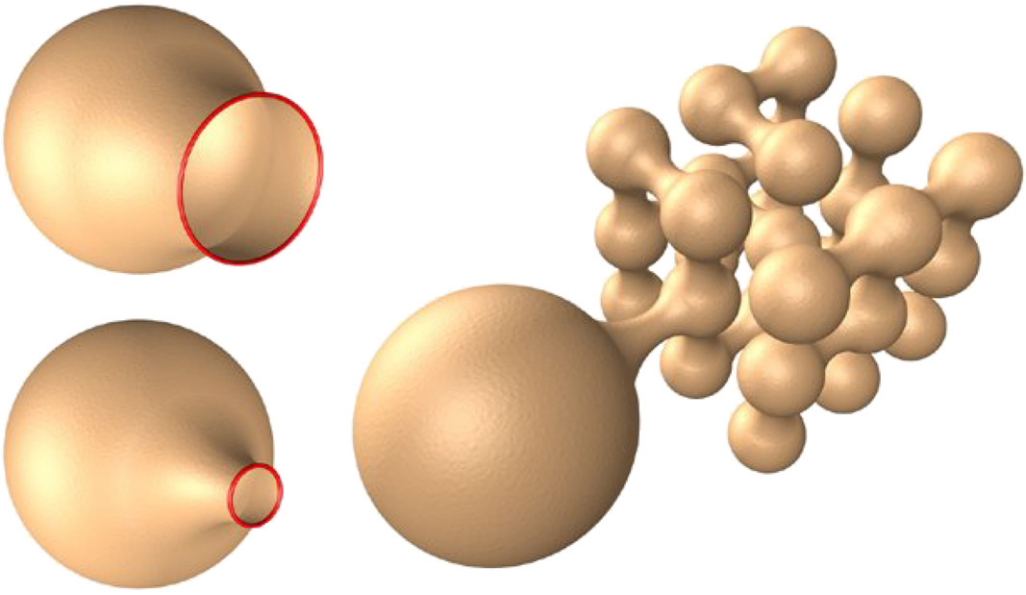

Fig. 21. Multiresolution surface development.

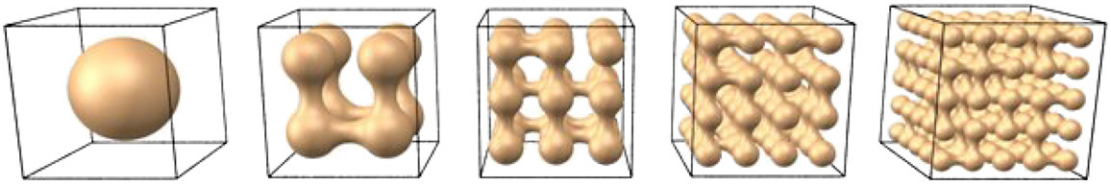

Fig. 22. Truchet surfaces fitted to cubic lattices $2 \times 2 \times 2$, $3 \times 3 \times 3$, $4 \times 4 \times 4$, $5 \times 5 \times 5$ and $6 \times 6 \times 6$.

contain no smaller Truchet surfaces within their volume. No point contained within the surface's volume will ever be more than r distance from the surface and the curvature of the surface will never exceed $1/r$ at any point. Unlike the two-dimensional case, however, the surface's complement does not share all of these properties, and points within the complement will not necessarily lie within r distance of the surface.

Truchet surface area (A_{ts}) and volume (V_{ts}) can be expressed neatly in terms of base radius r and number of ST vertices V as follows (full derivations are provided in Appendices A and B):

$$A_{ts} = \pi r^2(\sqrt{2}\pi(V-1)+4), \tag{8}$$

$$V_{ts} = \frac{1}{3}\pi r^3\left(\frac{1}{\sqrt{2}}(V-1)(16-3\pi)+4\right). \tag{9}$$

Fig. 22 shows a number of Truchet surfaces fitted to cubic lattices of increasing resolution, and Fig. 23 shows the relationship between surface area and volume for these surfaces. The characteristics of the graph are similar to the graph of Fig. 10, with volume approaching a constant percentage of the bounding box volume and surface area approaching a linear increase.

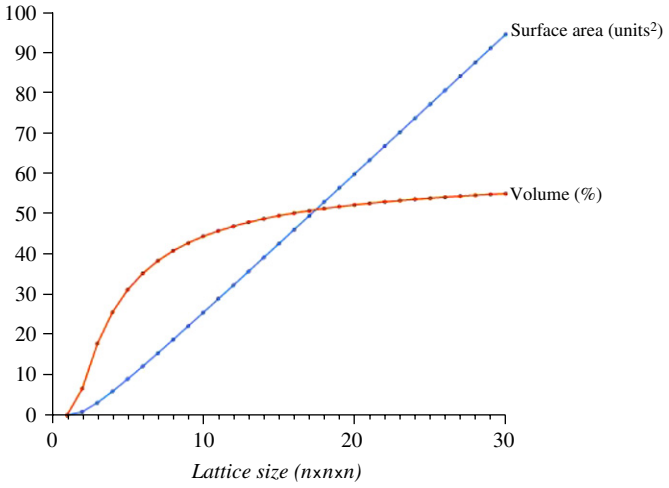

Fig. 23. Graph of surface area and volume for cubic lattices up to $30 \times 30 \times 30$.

9. Other dimensions

In closing, we consider the extrapolation of Truchet tiling to other dimensions. One-dimensional Truchet tiles might consist of two points which may or may not be

joined by a line segment, yielding two tile states. A composite shape randomly built from such tiles would form a series of line segments (a *Truchet dash*?) for which the distinction between inside and outside might depend on whether a given point falls within a line segment or not.

The four-dimensional case is more interesting but harder to visualize. An obvious choice for tiling unit would be the hypercube and an obvious choice for base lattice would be the polyhypercube, however the actual geometries of the tiles and the resulting composite shapes (especially defining their inside and outside) remain open questions.

10. Conclusions

This paper presents an algorithm for generating spanning tree contours, a special class of Truchet contour based on a random spanning tree of a Truchet tiling's underlying graph. Such contours are well defined and have some attractive properties, especially known minimum curvature, known maximum distance to the boundary for any contained point, and good ratios of perimeter length to area.

The technique is extended to multiresolution contours that may be used for image halftoning, and to three dimensions to define Truchet surfaces with similar properties.

Acknowledgements

Many thanks to Alan Tonisson for his input regarding the combinatorial aspects of Truchet tilings, and to Ken Brakke for his generous time and advice in relation to the diagonal neck intersection problem. Thanks to Bill Taylor and the anonymous reviewers for corrections and useful suggestions.

Appendix A. Calculation of Truchet surface area

Fig. 24 shows the geometry of a neck joining two spheres a and b of radius r, with centers situated $2\sqrt{2}r$ units apart. The circles c and d, also of radius r, are slices through the torus that encloses the neck. Note that this cross-sectional slice through the neck itself forms a Truchet tile within the square defined by the centres of a–d.

The surface area A_s of a sphere of radius r and the surface area A_c of the spherical cap clipped off where a neck meets the sphere are given by

$$A_s = 4\pi r^2, \tag{A.1}$$

$$\begin{aligned} A_c &= 2\pi r(r - \sqrt{2}r/2) \\ &= \pi r^2(2 - \sqrt{2}). \end{aligned} \tag{A.2}$$

Pappus's First Centroid Theorem [16] states that the surface area of a surface of revolution is given by the product of the arc length of the generating curve and the distance travelled by its geometric centroid, and can be used to determine the surface area of each neck. The generating curve in this case will be the circular arc centred at c (Fig. 24, left) swept around the axis containing a and b. Fig. 24 (right) shows this generating arc relative to the neck's central origin O. The generating arc's length L_a and its geometric centroid d_a relative to O are given by

$$L_a = \pi r/2, \tag{A.3}$$

$$c = \sqrt{2}r, \tag{A.4}$$

$$\begin{aligned} d_a &= c - \frac{r \sin\left(\frac{\theta}{2}\right)}{\frac{\theta}{2}} \\ &= \sqrt{2}r - \frac{r \sin\left(\frac{\pi}{4}\right)}{\frac{\pi}{4}} \\ &= \sqrt{2}r - \frac{4r}{\sqrt{2}\pi} \\ &= \frac{1}{\pi}\sqrt{2}r(\pi - 2). \end{aligned} \tag{A.5}$$

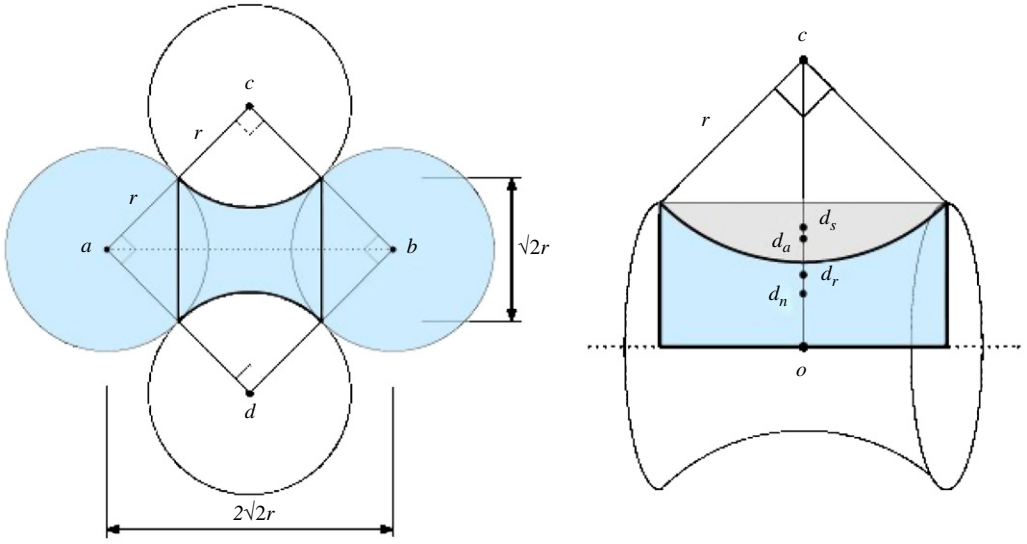

Fig. 24. Neck geometry (left) and neck construction as a surface of revolution (right).

The neck surface area A_n is therefore given by Pappus's First Theorem as follows:

$$\begin{aligned} A_n &= L_a 2\pi d_a \\ &= \frac{\pi r}{2} 2\pi \frac{1}{\pi}\sqrt{2}r(\pi-2) \\ &= \sqrt{2}\pi r^2(\pi-2). \end{aligned} \tag{A.6}$$

The total surface area A_{ts} of a Truchet surface created from V vertices and E edges will be the sum of the surface area of V spheres and E necks minus the surface area of the two spherical caps clipped off per neck. Hence

$$\begin{aligned} A_{ts} &= VA_s + E(A_n - 2A_c) \\ &= V4\pi r^2 + (V-1)(\sqrt{2}\pi r^2(\pi-2) - 2\pi r^2(2-\sqrt{2})) \\ &= \pi r^2(4V + (V-1)(\sqrt{2}\pi - 2\sqrt{2} - 4 + 2\sqrt{2})) \\ &= \pi r^2(4V + \sqrt{2}\pi V - 4V - \sqrt{2}\pi + 4) \\ &= \pi r^2(\sqrt{2}\pi(V-1) + 4). \end{aligned} \tag{8 − restated}$$

Appendix B. Calculation of Truchet surface volume

V_s the volume of a sphere of radius r and V_c the volume of the spherical cap clipped off where a neck meets the sphere are given by

$$V_s = \tfrac{4}{3}\pi r^3, \tag{B.1}$$

$$\begin{aligned} V_c &= \frac{1}{3}\pi r^3\left(2 - 3\sin\left(\frac{\pi}{4}\right) + \sin^3\left(\frac{\pi}{4}\right)\right) \\ &= \frac{1}{3}\pi r^3\left(2 - \frac{3}{\sqrt{2}} + \frac{1}{\sqrt{2^3}}\right) \\ &= \frac{1}{12}\pi r^3(8 - 5\sqrt{2}). \end{aligned} \tag{B.2}$$

Neck volume V_n can be calculated using Pappus's Second Centroid Theorem [16] which states that the volume of a solid of revolution is given by the product of the area of the generating lamina and the distance travelled by its geometric centroid. The generating lamina for the neck is the area shaded blue in Fig. 24 (right) formed by the indicated rectangle minus the circular segment centred at c with $\theta = 90°$. The distance d_r from the origin O to the rectangle's geometric mean and the distance d_s from the origin O to the circular segment's geometric mean are given by

$$d_r = \frac{\sqrt{2}r}{4}, \tag{B.3}$$

$$\begin{aligned} d_s &= c - \frac{4r\sin^3\left(\frac{\theta}{2}\right)}{3(\theta - \sin\theta)} \\ &= \sqrt{2}r - \frac{4r\sin^3\left(\frac{\pi}{4}\right)}{3\left(\frac{\pi}{2} - \sin\left(\frac{\pi}{2}\right)\right)} \\ &= r\left(\sqrt{2} - \frac{\frac{4}{\sqrt{2^3}}}{3\left(\frac{\pi}{2}-1\right)}\right) \\ &= \sqrt{2}r\left(1 - \frac{2}{3(\pi-2)}\right). \end{aligned} \tag{B.4}$$

The areas of the rectangle (A_r), circular segment (A_s) and the neck's generating lamina (A_{nl}) are

$$\begin{aligned} A_r &= \sqrt{2}r\frac{\sqrt{2}r}{2} \\ &= r^2, \end{aligned} \tag{B.5}$$

$$\begin{aligned} A_s &= \frac{r^2}{2}\left(\frac{\pi}{2} - \sin\left(\frac{\pi}{2}\right)\right) \\ &= \frac{r^2}{2}\left(\frac{\pi}{2} - 1\right) \\ &= \frac{1}{4}r^2(\pi-2), \end{aligned} \tag{B.6}$$

$$\begin{aligned} A_{nl} &= A_r - A_s \\ &= r^2 - \frac{1}{4}r^2(\pi-2) \\ &= \frac{1}{4}r^2(6-\pi). \end{aligned} \tag{B.7}$$

The distance d_n from the origin O to the geometric centroid of the neck's generating lamina can then be calculated as follows:

$$\begin{aligned} d_n &= \frac{d_r A_r - d_s A_s}{A_{nl}} \\ &= \frac{\frac{\sqrt{2}r}{4}r^2 - \sqrt{2}r\left(1 - \frac{2}{3(\pi-2)}\right)\frac{1}{4}r^2(\pi-2)}{\frac{1}{4}r^2(6-\pi)} \\ &= \frac{\sqrt{2}r - \sqrt{2}r\left(1 - \frac{2}{3(\pi-2)}\right)(\pi-2)}{(6-\pi)} \\ &= \frac{\sqrt{2}r\left(1 - \left(\pi - 2 - \frac{2}{3}\right)\right)}{(6-\pi)} \\ &= \frac{\sqrt{2}r\left(\frac{11}{3} - \pi\right)}{(6-\pi)}. \end{aligned} \tag{B.8}$$

By Pappus's Second Theorem, the volume V_n of a neck with flat ends will be

$$\begin{aligned} V_n &= A_n 2\pi d_n, \\ &= \frac{1}{4}r^2(6-\pi)2\pi\frac{\sqrt{2}r\left(\frac{11}{3} - \pi\right)}{(6-\pi)} \\ &= \frac{1}{\sqrt{2}}\pi r^3\left(\frac{11}{3} - \pi\right). \end{aligned} \tag{B.9}$$

The final volume V_{ns} of a neck with each end scooped out by a spherical cap of radius r (the volumetric equivalent to the dark blue region in Fig. 8, right) will be

$$\begin{aligned} V_{ns} &= V_n - 2V_c \\ &= \frac{1}{\sqrt{2}}\pi r^3\left(\frac{11}{3} - \pi\right) - 2\frac{1}{12}\pi r^3(8 - 5\sqrt{2}) \\ &= \frac{1}{\sqrt{2}}\pi r^3\left(\frac{11}{3} - \pi - \frac{4\sqrt{2}}{3} + \frac{5}{3}\right) \\ &= \frac{1}{3}\pi r^3\left(\frac{1}{\sqrt{2}}(16 - 3\pi) - 4\right). \end{aligned} \tag{B.10}$$

The volume V_{ts} of a Truchet surface created from V vertices and E edges (where $E = V-1$) will therefore be the total volume of V spheres plus E scooped necks as follows:

$$\begin{aligned} V_{ts} &= VV_s + EV_{ns} \\ &= V\frac{4}{3}\pi r^3 + (V-1)\frac{1}{3}\pi r^3\left(\frac{1}{\sqrt{2}}(16-3\pi)-4\right) \\ &= \frac{1}{3}\pi r^3\left(4V + (V-1)\left(\frac{16}{\sqrt{2}} - \frac{3\pi}{\sqrt{2}} - 4\right)\right) \\ &= \frac{1}{3}\pi r^3\left(\frac{1}{\sqrt{2}}(V-1)(16-3\pi)+4\right). \qquad (9-\text{restated}) \end{aligned}$$

Code listings

1. Define a grid of square cells fitted to the target area
2. Mark all cells as unvisited
3. while (any 2×2 group of cells remains unvisited)
   {
   3.a Find the largest graph G of alternating 2×2 intersections
   3.b Choose a random spanning tree of G
   3.c Apply tree-to-contour replacement rules to generate a contour
   3.d Mark visited cells
   }

Listing 1. Algorithm for generating area-filling ST contours.

```
#declare r = 1;          // base radius
#declare s = 2*sqrt(2)*r;      // unit spacing

merge
{// surface
   sphere { <0, 0, 0> r }          // vertex 0
   sphere { <s, 0, 0> r }          // vertex 1
   difference
   {// neck
      cylinder { <0, 0, 0> <s, 0, 0> s/4 }
      torus { s/2 r rotate <90, 90, 0>translate<s/2, 0,
      0> }
   }
}
```

Listing 2. POV-Ray code for describing the three-dimensional dumbbell as a CSG object.

References

[1] Smith C, Boucher P. The tiling patterns of Sebastian Truchet and the topology of structural hierarchy. Leonardo 1987;20(4):373–85.

[2] Weisstein E. Truchet tiling. 〈http://mathworld.wolfram.com/TruchetTiling.html〉.

[3] Pickover C. Picturing randomness with Truchet tiles. Computers, pattern, chaos, and beauty: graphics from an unseen world. New York: S.t Martin's Press; 1990. p. 329–32.

[4] Gale D, Propp J, Sutherland S, Troubetzkoy S. Further travels with my ant. Mathematical Intelligencer 1995;17:48–56.

[5] Pasechnik D, Weisstein E. Jordan curve theorem. 〈http://mathworld.wolfram.com/JordanCurveTheorem.html〉.

[6] Sillke T. Expected number of pattern in a matrix. 〈http://www.math.uni-bielefeld.de/~sillke/PUZZLES/truchet_tiles〉.

[7] Broder A. Generating random spanning trees. In: 30th annual symposium on foundations of computer science, Research Triangle Park. North Carolina: IEEE Press; 1989. p. 442–7.

[8] Duplantier B. Hull percolation and standard percolation. Journal of Physics A: Mathematical and General 1988:3969–73.

[9] Smith D. Welcome to the world of trax. 〈http://www.traxgame.com/about.php〉.

[10] Berlekamp E, Conway J, Guy R. Winning ways for your mathematical plays, games in particular, vol. 2. London: Academic Press; 1982.

[11] Bosch R, Herman A. Continuous line drawings via the traveling salesman problem. Operations Research Letters 2004;32(4):302–3.

[12] Chan K. Tangle series and tanglegrams: a new combinatorial puzzle. Journal of Recreational Mathematics 2002;31(1):1–11.

[13] Huff K. 3D Truchet tiling. 〈http://home4.inet.tele.dk/ibras/truchet.htm〉.

[14] Bourke P. Truchet tiles in 2D and 3D. 〈http://local.wasp.uwa.edu.au/~pbourke/texture_colour/periodic/〉.

[15] Brakke K. The surface evolver. 〈http://www.susqu.edu/facstaff/b/brakke/evolver/〉.

[16] Weisstein E. Pappus's centroid theorem. 〈http://mathworld.wolfram.com/PappussCentroidTheorem.html〉.